Optics & Laser Technology 57 (2014) 293–303

Contents lists available at ScienceDirect

Optics & Laser Technology

journal homepage: www.elsevier.com/locate/optlastec

Lens sag and diameter measurement of large-size microlenses using sub-pixel algorithm and optical interferometry

Shir-Kuan Lin, Shih-Wei Yang *

Institute of Electrical and Control Engineering, National Chiao Tung University, Hsinchu, Taiwan

ARTICLE INFO

Available online 5 July 2013

Keywords:
Diameter
Lens sag
Large-size microlens

ABSTRACT

In this paper, an automatic optical inspection system is designed specifically to measure the diameter and lens sag of large-size microlenses: 1. The proposed algorithm of measuring lens diameter locates the lens center through the Euclidean distance array, and determines the lens edge along an initiated ray using linear interpolation with sub-pixel accuracy. 2. The lens sag is calculated from a single fringe pattern of large-size microlens, in combination with the measured lens diameter. 3. According to the experiment results, the proposed system has advantages of high applicability, rapid processing speed, and good accuracy with the RMS error≤1% of measuring a large-size microlens, but without the requirement of prior training. The system architecture of non-contact measurement would not cause scratches on the lens surface and is inexpensive, thus, which is particularly suitable for the in-line inspection of industry field.

1. Introduction

Due to increasingly advanced semiconductor manufacturing technology, microlens molds can be produced by electroforming and became easy to be reproduced. However, poor mold manufacturing and non-uniform thermal expansion and contraction will cause defects in the microlens. Hence, an automatic optical inspection (AOI) system for measuring the diameter and les sag of a large-size microlens is developed in this study. The current methods to measure the size of microlens can be divided into contact measurement and non-contact measurement. The contact measurement is carried by scanning electron microscope (SEM), atomic force microscope (AFM), and stylus profiler [1–3], which are very expensive, tend to cause scratches on the surface of the microlens, and have low measurement speed. Hence, the non-contact measurement method is adopted in this study.

When lens sag is similarly equal to the wavelength of the light source, the interference fringes of the microlens are sparsely distributed and can be clearly observed; therefore, the surface profile of a microlens can be accurately measured through interferometry [4–7]. A 3D profile of such microlens can be reconstructed using the grating projection techniques [8–10] or Fast Fourier Transform methods [11,12]. However, when lens sag is far greater than the wavelength of the light source, only a few central circular fringes of the microlens are clearly distributed, and the surrounding fringes are blurred and difficult to identify due to very high distribution density. Thus, the above method is not suitable for measuring the lens sag of large-size microlenses. Yang et al. [13] calculated the microlens center using the center of area method (COA), then calculated the microlens sag according to the desired diameter. However, the actual diameter is not measured, thus errors existed in the obtained lens sag.

As the lens sag is much larger than the light wavelength, a fuzzy area often arises at the circular edge of large-size microlens, which is due to the low contrast, and the edge points of microlens is unable to be accurately determined. Although there have been many edge detectors proposed [14,15], but they cannot be applied to obtain good results for the circular edge of microlenses. In other words, the diameter of the microlens cannot be directly calculated. The fuzzy theory is also often used for edge analysis [16,17]. Lin et al. [18] determined the edge location of a microlens using fuzzy ratio analysis in order to measure the diameter of the microlens, but the results were easily affected by noise in the image.

To improve the above drawbacks, an innovative method, which combines with the concept of sub-pixel [19,20], is proposed specifically for measuring the diameter of a large-size microlens. Moreover, a second method is designed based on the adaptive neuro-fussy inference system (ANFIS) [21] to verify the superiority and practicality of the proposed sub-pixel algorithm. For measuring the lens sag of a large-size microlens, a mathematical model for rapid estimation of lens sag is also established, and the calculated diameter can be used to determine the microlens sag. By integrating the algorithms for diameter and sag measurement, the proposed AOI system is established with the advantage of fast

* Corresponding author. Tel.: +886 3 5712121x54423.
E-mail address: swyang.nctu@msa.hinet.net (S.-W. Yang).

0030-3992/$ - see front matter © 2013 Elsevier Ltd. All rights reserved.
http://dx.doi.org/10.1016/j.optlastec.2013.06.002

measurement and is particularly suitable for the large-size microlens inspection of industry field.

2. Methods of lens sag and diameter measurement of large-size microlenses

In order to highlight the edge contour of large-size microlenses, a backlight module is used as the light source in this study, as shown in Fig. 1. The sharpness of the circular edge of a microlens is far lower than that of the straight edge; thus, a series of image processing algorithms are proposed to solve this problem. The detailed process is described in the following sections.

2.1. Positioning of microlens center

To measure the diameter, the coordinates of microlens center are calculated first. As dust and other foreign matters may attach to microlens samples, or due to processing defects, the image of a microlens contains noise. The edge contour of the microlens will then be broken and incomplete after binaryzation and filtering operations. In order to solve this problem, a max inscribed circle of the binary image of a microlens is found, and the center of this circle is approximate to the microlens center, which can avoid noise interference.

Assuming the captured image is an $n \times m$ image, and the black pixels of binaryzation are defined as the basis points. There are a total of r basis points, and the $n \times m$ Euclidean distance matrix **D** can be defined as follows:

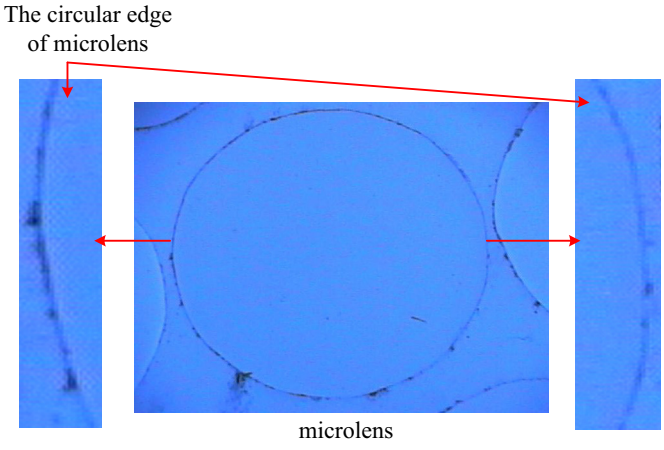

Fig. 1. Image of microlens edge.

$$\mathbf{D} = \begin{bmatrix} d_{11} & d_{12} & \cdots & d_{1(n-1)} & d_{1n} \\ d_{21} & d_{22} & \cdots & d_{2(n-1)} & d_{2n} \\ \vdots & \vdots & \ddots & \vdots & \\ d_{(m-1)1} & d_{(m-1)2} & \cdots & d_{(m-1)(n-1)} & d_{(m-1)n} \\ d_{m1} & d_{m2} & \cdots & d_{m(n-1)} & d_{mn} \end{bmatrix} \tag{1}$$

$$d_{ij} = \min_{r}\left(\sqrt{(j-x_{bk})^2 + (i-y_{bk})^2}\right),\ i = 1,2,\ldots,m;\ j = 1,2,\ldots,n;\ k = 1,2,\ldots,r \tag{2}$$

where, d_{ij} is the element in ith row and jth column of Euclidean distance array **D**, and shows the distance from pixel (j,i) to the nearest basis point(x_{bk},y_{bk}).

The value of each element in matrix **D** is calculated by Eq. (2). After the Euclidian distance matrix is obtained according to the binaryzation result, the position of the maximum value in the matrix is the center of the max inscribed circle of the binary image, which can be considered as the microlens center, and the maximum value is the radius of the max inscribed circle. The value of each element in the matrix is normalized from 0 to 255, and the red point represents the positioning result of microlens center C, as shown in Fig. 2.

2.2. Lens diameter measurement using the concept of a sub-pixel

An initiated ray is made along the edge direction of a microlens with center coordinate $C(x_c,y_c)$ as the starting point, and is rotated each time by fixed angle θ for 360° scanning. $P(x_p,y_p)$ is any point on the initiated ray, as shown in Fig. 3(a), and its coordinate can be expressed as [6]

$$\begin{cases} x_p = x_c + \Delta l \\ y_p = y_c + \Delta l \times \tan\theta \end{cases} \tag{3}$$

where, $\Delta l > 0$ and $\theta \in [0^\circ, 360^\circ)$.

Consider that any point $P(x_p,y_p)$ on the initiated ray must be adjacent to two other pixels, as shown in Fig. 3(b), thus, the gradient G_p of $P(x_p,y_p)$ is defined as

$$G_p = \max(G_1, G_2) \tag{4}$$

where, G_1 and G_2 are the gradient of $P(x_p,y_p)$ and two adjacent pixels, respectively.

According to Eq. (4), the gradients of all pixels on the initiated ray can be calculated. Two points with the maximum gradient are found on this initiated ray, and one of the two points, with a low gray value, is defined as the "initial edge point". For filtering out the improper results of searching the initial edge points, the distance x_{di} from each initial edge point to the microlens center is respectively calculated, and then sequenced in an ascending

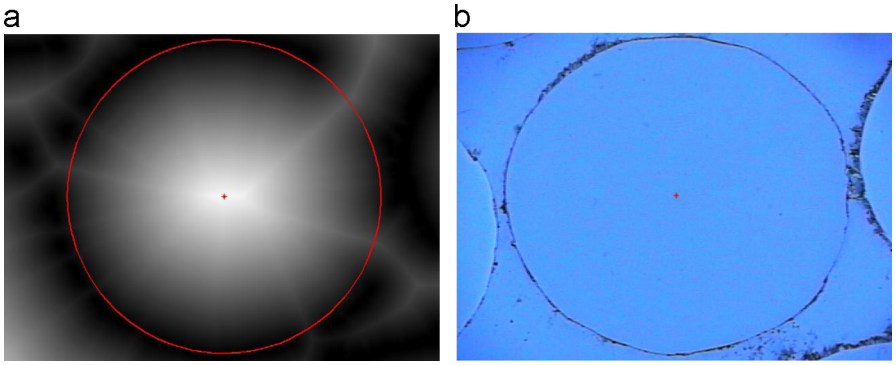

Fig. 2. Result of the maximum inscribed circle and microlens center positioning. (a) Result of Euclidean distance matrix and (b) Result of microlens center positioning.

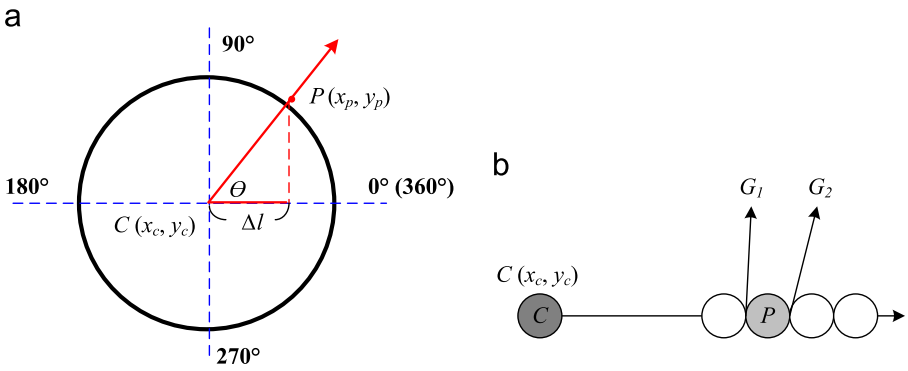

Fig. 3. There is an initial edge point on every initiated ray. (a) An initiated ray at fixed angle θ and (b) The definition of gradient in this paper.

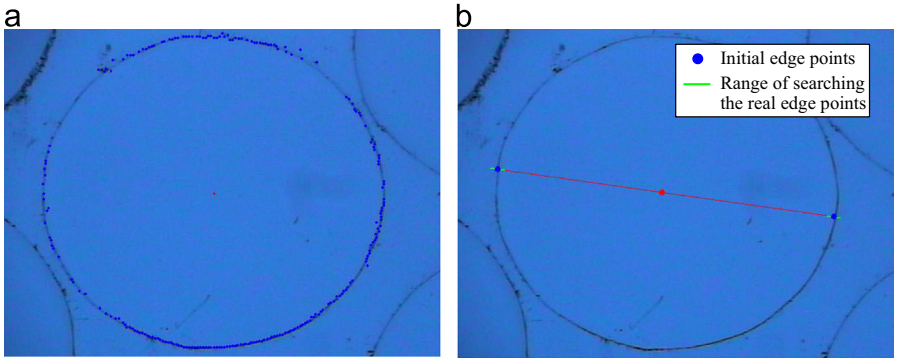

Fig. 4. Range of searching the actual edge points, as decided by the initial edge points. (a) Result of searching initial edge points and (b) Range of searching the real edge points.

order, so as to obtain the median distance $x_{d-median}$. Reasonable initial edge points must meet the following conditions

$$x_{d-median}-\Delta t < x_{di} < x_{d-median}+\Delta t,\ i=1,2,\ldots,360 \tag{5}$$

where, x_{di} is the distance from the initial edge point on the ith initiated ray to the microlens center, and Δt is a threshold value (a positive integer).

Hence, points that do not conform to Eq. (5) should be eliminated. The filtering results of the initial edge points is shown in Fig. 4(a), and the blue points are the initial edge points and the red point is the microlens center.

The initial edge points in Fig. 4(a) have the characteristics of high gradients; however, the image contains many noises, thus, these initial edge points may not be the actual edge points of the microlens. Selecting any two initial edge points in Fig. 4(a), which are respectively located on the initiated ray at angle θ and angle (θ +180°) (Fig. 3(a)); extend u pixels inward and outward along the initiated ray with the two initial edge points as the center, respectively; regard the ($2u$+1) pixels as the range for searching the actual edge points, as shown in Fig. 4(b). The Laplacian of Gaussian operation (LoG) [22] is applied to the ($2u$+1) pixels, and the Gaussian filtering is carried out first

$$f_{gausssian}=f(x,y)g'(x,y) \tag{6}$$

$$g'(x,y)=e^{-((x^2+y^2)/2\sigma^2)}$$

where, $f_{gausssian}$ is the filtering result, $f(x,y)$ is the gray value of input pixel, σ is the standard deviation, and $g'(x,y)$ is the Gaussian filter.

The second derivative of each pixel is then calculated

$$\begin{aligned} f_{LoG} &= \nabla^2 f_{gausssian} \\ &= [\nabla^2 g'(x,y)]f(x,y) \end{aligned} \tag{7}$$

$$\nabla^2 g'(x,y)=\frac{1}{\pi\sigma^4}\left[\frac{x^2+y^2}{2\sigma^4}-1\right]e^{-((x^2+y^2)/2\sigma^2)}$$

where, f_{LoG} is the second derivative of pixel $f(x,y)$, σ is the standard deviation, and $\nabla^2 g''(x,y)$is the LoG operator.

The computing result of Eq. (7) can be approximated by the following mask operation

$$\mathbf{M}_{LoG}=\begin{bmatrix} 0 & 0 & -1 & 0 & 0 \\ 0 & -1 & -2 & -1 & 0 \\ -1 & -2 & 16 & -2 & -1 \\ 0 & -1 & -2 & -1 & 0 \\ 0 & 0 & -1 & 0 & 0 \end{bmatrix} \tag{8}$$

Let u=10, the results of the mask operation (Eq. (8)) of the two ranges (42 pixels) in Fig. 4(b) are sequenced in the direction from the inside of the lens to the lens edge, as shown in Fig. 5.

The edge points of the microlens must be located at the zero crossing of the second derivative. Taking the LoG result of right edge in Fig. 5 as an example: find the maximum and minimum values of the second derivative in the search range, let the extreme coordinate closer to microlens center C be (x_2,y_2,z_2) and another extreme coordinate be(x_1,y_1,z_1), and then redraw the coordinates in the three-dimensional coordinate system, as shown in Fig. 6. According to the principle of linear interpolation, coordinate $E(x_e, y_e)$ of the microlens edge points on the initiated ray at angle θ can be expressed as

$$\begin{cases} x_e = x_2 + \mathbf{sgn}[\cos\theta]|x_1-x_2|\frac{|z_2|}{|z_1-z_2|} \\ y_e = y_2 - \mathbf{sgn}[\sin\theta]|y_1-y_2|\frac{|z_2|}{|z_1-z_2|} \end{cases} \tag{9}$$

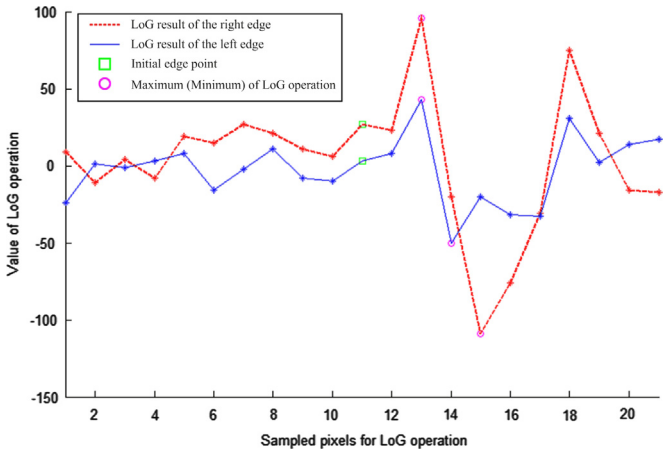

Fig. 5. Results of LoG operation of the two ranges in Fig. 4(b).

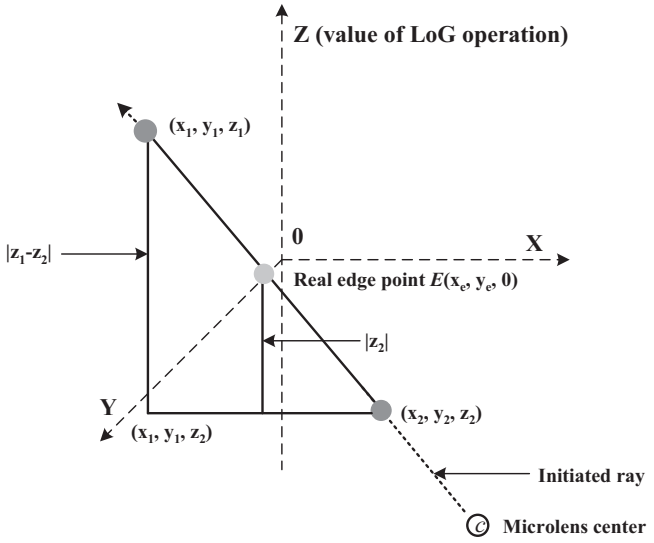

Fig. 6. Calculation of the actual edge point by the sub-pixel technique.

$$\mathbf{sgn}[f]=\begin{cases}1, & \mathbf{if} f>0\\ 0, & \mathbf{if} f=0\\ -1, & \mathbf{if} f<0\end{cases}$$

where, f is a real number, and $\theta\in[0^\circ, 360^\circ)$.

Similarly, coordinate $E'(x'_e,y'_e)$of another edge point on the initiated ray at angle $(\theta+180^\circ)$ can be obtained. The diameter h_D of the microlens can be expressed as

$$h_D=\Delta s\times\sqrt{(x_e-x'_e)^2+(y_e-y'_e)^2} \tag{10}$$

where, Δs is the actual length of a pixel in the image.

The measurement of diameter only requires the LoG operation of $(2u+1)$ pixels, thus, the computation is greatly simplified, and complex computation of the traditional LoG method is effectively improved.

2.3. Lens diameter measurement using ANFIS model

The ANFIS architecture proposed by Jang [21] is adopted as the second method to measure microlens diameter. The gradient of an image is selected as the input of ANFIS. However, in order to avoid being influenced by image noise, the gray value of the image is used in as another input of ANFIS. The performance of the ANFIS model depends on whether the training data is correctly selected. Therefore, the microlens edge points are selected manually, and these points are known as the optimal edge points. The suboptimal edge point and the worst edge point can be further selected on the line connecting each optimal edge point and lens center, as shown in Fig. 7(a). Three hundred groups of optimal edge points, suboptimal edge points, and worst edge points, are selected from one image as the training data of ANFIS, as shown in Fig. 7(b).

The gradients of the optimal edge point set, suboptimal edge point set, and worst edge point set can all be calculated using Eq. (4), and their gray values can be simultaneously recorded. These two inputs correspond to a score between 1 and −1 as the output of ANFIS. A higher score indicates that the point is more likely to be the actual edge point. In this study, the weight ratio of the gradient to the gray value is set as 2:1. When the gradient is higher, and the gray value is closer to the average value, the score should be higher. Thus, the score of the optimal edge point can be defined as

$$Score_{B_i}=0.34+\left(0.44\times\frac{G_i}{G_{B\max}}\right)+\left[0.22\times\left(1-\frac{|f_i-f_{Bavg}|}{|\Delta f_{\max}|}\right)\right],\quad i=1,2,\ldots,n \tag{11}$$

where, $G_{B\max}$ is the maximum gradient among the optimal edge points, G_i is the gradient of the measured point, f_i is the gray value of the measured point, f_{Bavg} is the average gray value of the optimal edge points, $\Delta f_{\max}=\max_n(f_i-f_{Bavg})$, and n is the total number of optimal edge points.

The score of the suboptimal edge point can be defined as

$$Score_{M_i}=-0.34+0.45\times\frac{G_i}{G_{M\max}}+\left[0.23\times\left(1-\frac{|f_i-f_{Mavg}|}{|\Delta f_{\max}|}\right)\right],\quad i=1,2,\ldots,n \tag{12}$$

where, $G_{M\max}$ is the maximum gradient among the suboptimal edge points, f_{Mavg} is the average gray value of the suboptimal edge points, $\Delta f_{\max}=\max_n(f_i-f_{Mavg})$, and n is the total number of suboptimal edge points.

The score of the worst edge point can be defined as

$$Score_{S_i}=-1+0.44\times\frac{G_i}{G_{S\max}}+\left[0.22\times\left(1-\frac{|f_i-f_{Savg}|}{|\Delta f_{\max}|}\right)\right],\quad i=1,2,\ldots,n \tag{13}$$

where, $G_{S\max}$ is the maximum gradient among the worst edge points, f_{Savg} is the average gray value of the worst edge points, $\Delta f_{\max}=\max_n(f_i-f_{Savg})$, and n is the total number of worst edge points.

The gradients, gray values, and the corresponding scores of optimal, suboptimal, and worst training data are respectively input into MATLAB for training. The input partition is set as three, and the membership function is set as the bell distribution. The results are shown in Fig. 8(a). The obtained relation surface of inputs and outputs after training is shown in Fig. 8(b). The points with the highest scores on both ends of the initiated ray are the actual edge points, and the diameter of the microlens can be calculated using Eq. (10).

2.4. Lens sag measurement

The object measured in this study is a large-size microlens, and only a few central interference fringes can be observed. As the surrounding fringes are too densely distributed, they are blurred and difficult to identify in the image, as shown in Fig. 9. By modifying the method proposed in literature [13], a simpler result is obtained, which can quickly and accurately estimate lens sag, in combination with the microlens diameter measured in Section 2.2. Considering the principle of the Fizeau Interferometer, given that

$$h_S=\frac{{h_R}^2}{2R} \tag{14}$$

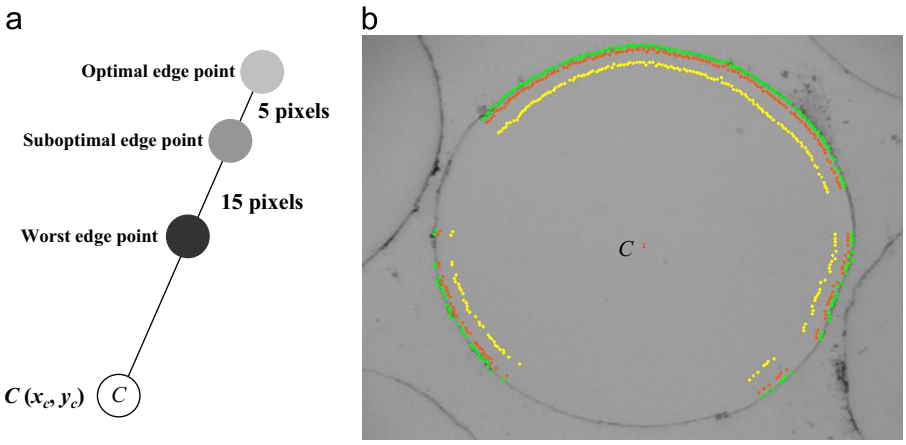

Fig. 7. Sampling method and results of training data. (a) Sampling method of training data and (b) Sampling result of training data.

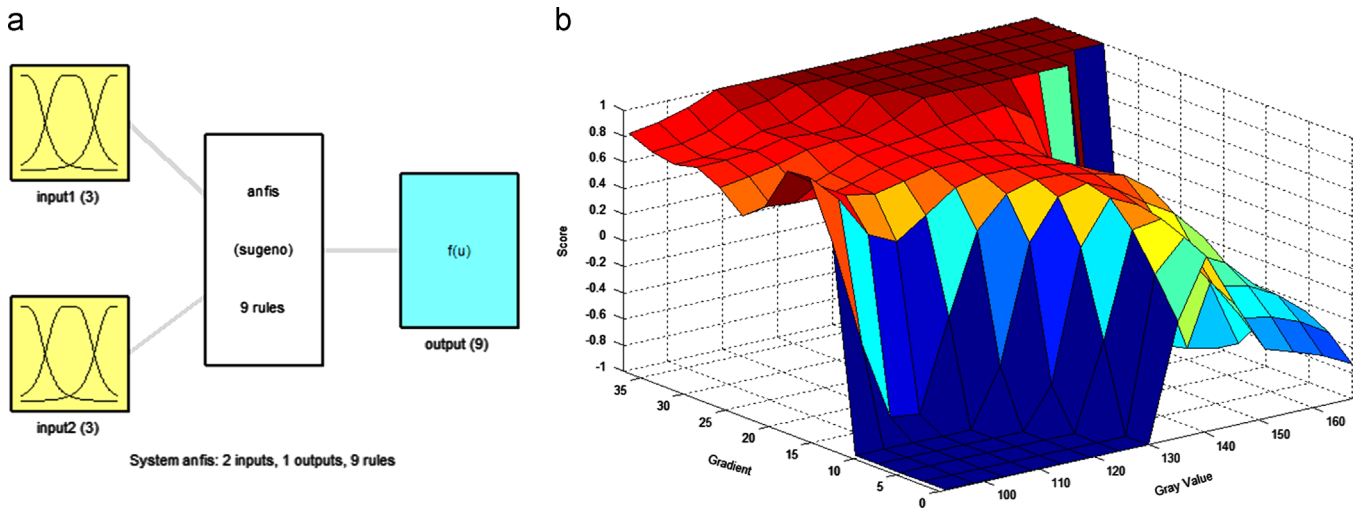

Fig. 8. Training results of ANFIS. (a) The obtained FIS structure after training and (b) Relation surface of inputs and outputs.

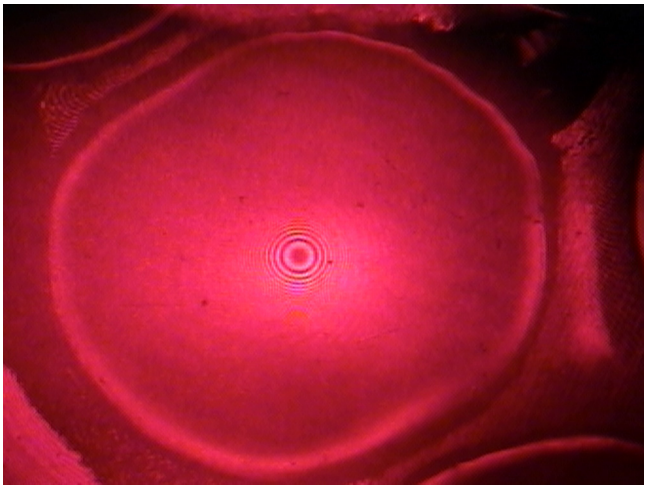

Fig. 9. Image of interference fringes in a large-size microlens.

where, R is the radius of microlens curvature, h_R is the microlens radius, $h_R = h_D/2$ and h_S is the lens sag.

Assuming that the central fringes are dark fringes ($m=0$), and the observed outermost fringe is the mth dark fringe. Then the air wedge of the mth dark fringe is $h_{S(m)} = m\lambda/2$, λ is the wavelength of the light source, and thus yielding $R = {d_m}^2/m\lambda$. The lens sag h_S can be calculated by substituting the value of R into Eq. (14)

$$h_S = \frac{{h_R}^2 m\lambda}{2{d_m}^2} = \frac{{h_D}^2 m\lambda}{8{d_m}^2} \tag{15}$$

According to Eq. (15), if the central fringe is a bright fringe, then the above process is changed to measure the distance from the lens center to the mth bright fringe, and the lens sag can still be calculated using Eq. (15), which does not affect the correctness of this algorithm.

3. Experimental results and discussion

3.1. Framework of the proposed AOI system

The experimental framework of proposed AOI system can be divided into two parts: in the first part, the microlens diameter is measured, and the equipments include CCD camera, objective lens set, and backlight module. The backlight module is used as the light source, which can highlight the edge features of a microlens, as shown in Fig. 10. In the second part, the lens sag is measured by using a diode laser as the light source, which transmits the light source into the microscope set with a fiber bundle and irradiates on the microlens surface through the coaxial light. The optical flat is placed on the microlens sample to form the Fizeau

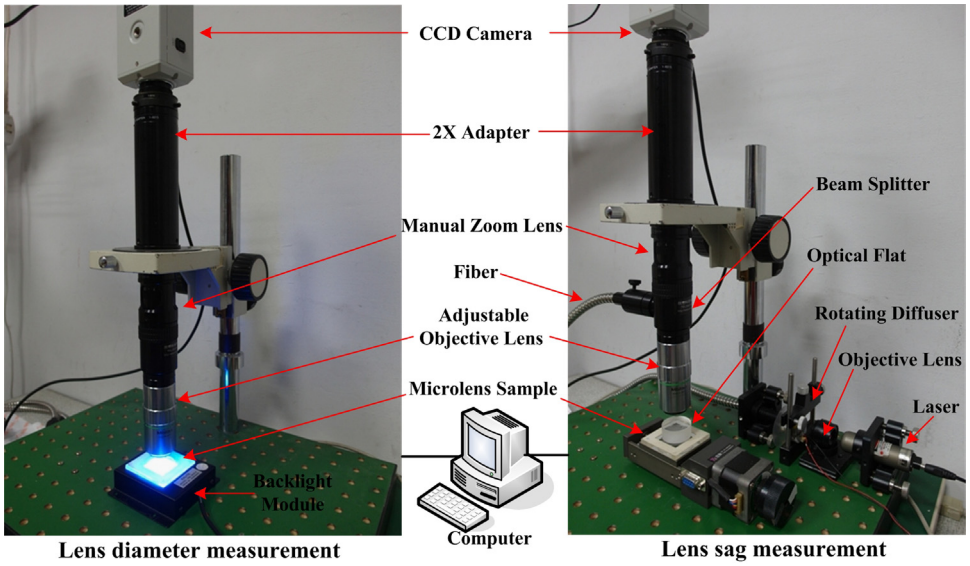

Fig. 10. System setup of the proposed AOI system.

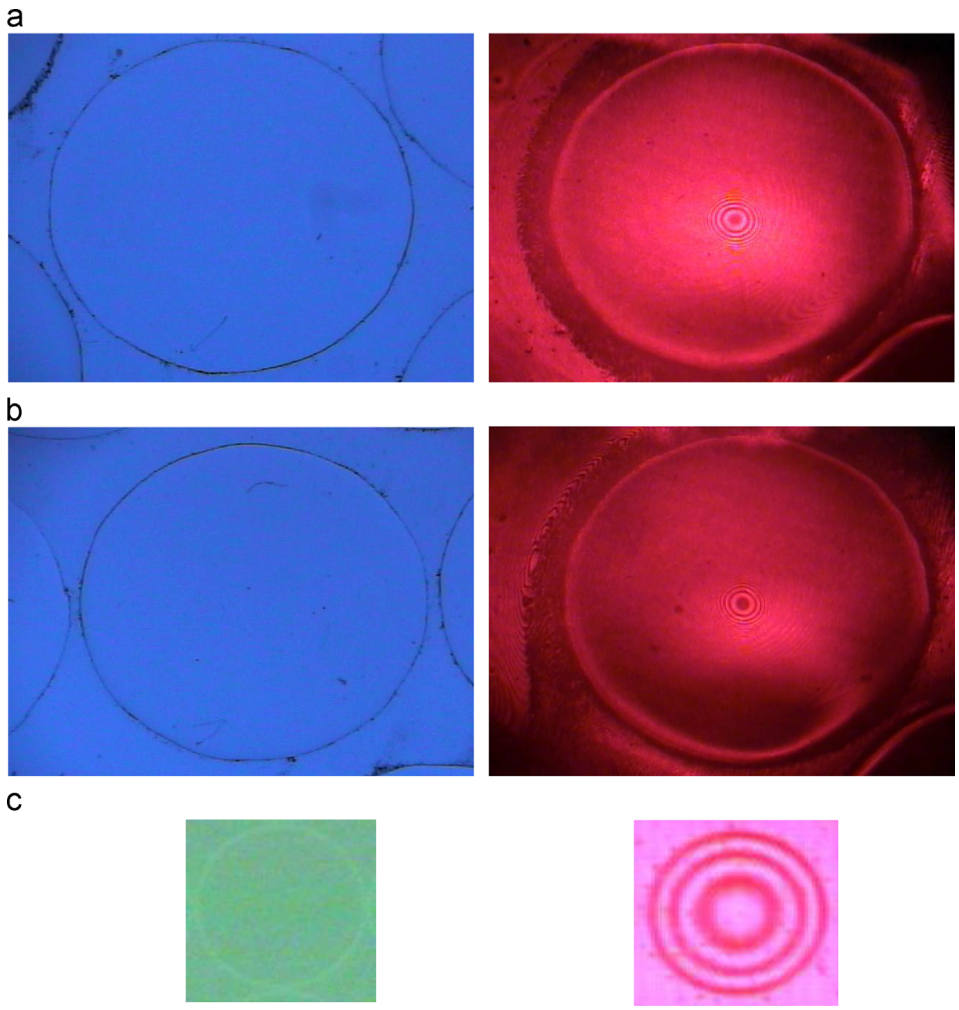

Fig. 11. Backlight images and interference images of three microlens samples. (a) Sample A with the diameter of 3648μm and sag of 75μm, (b) Sample B with the diameter of 3770μm and sag of 92μm and (c) Sample C with the diameter of 110μm and sag of 1μm.

interferometer for observing the interference image of the microlens. In order to improve the phenomenon of a non-uniform light field, an objective lens is used at the light source to expand the laser beam. A rotating diffuser [6] is installed for eliminating the laser speckles and improving the image quality. The overall architecture is as shown in Fig. 10.

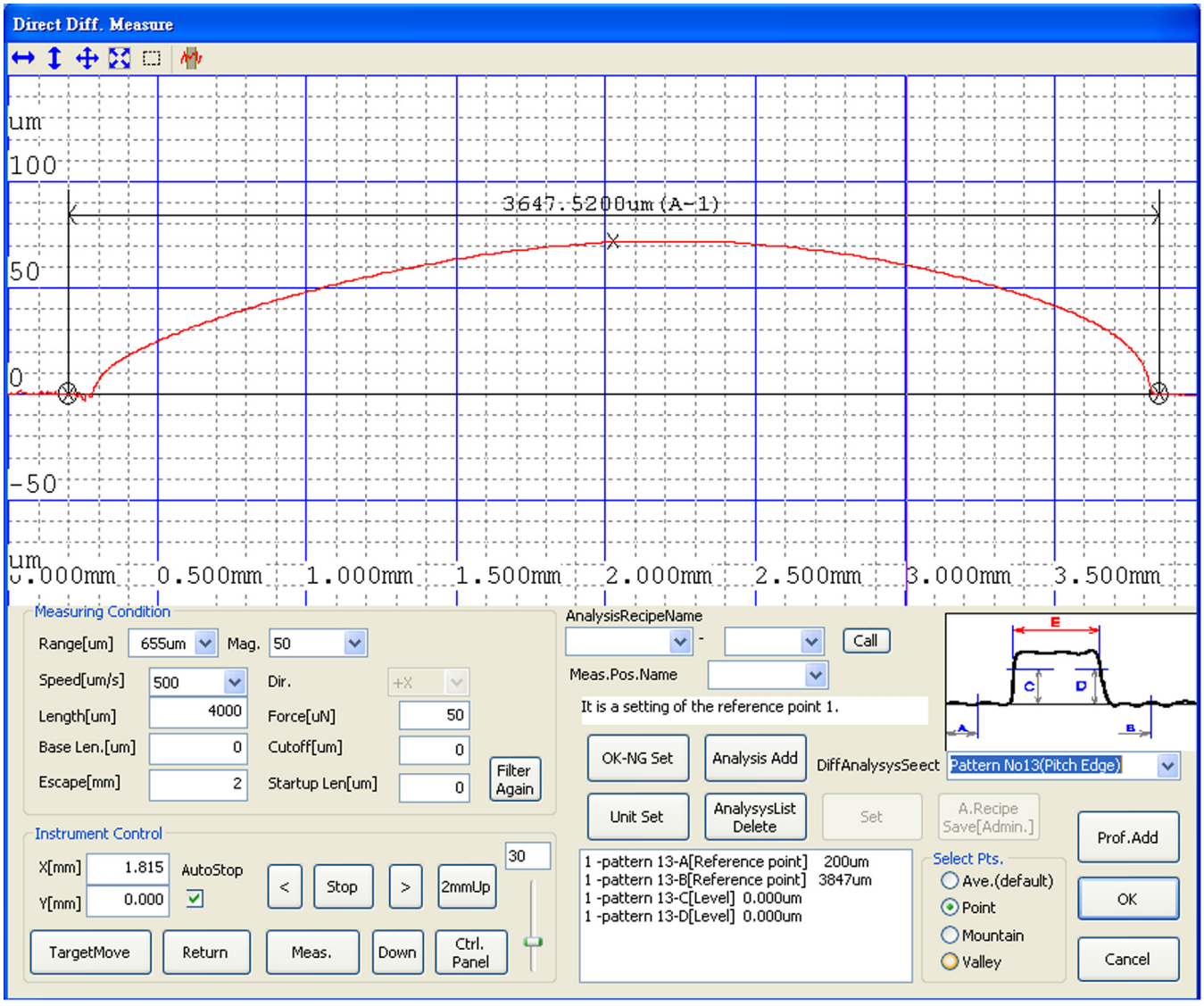

Fig. 12. Diameter measurement result of sample A by ET-3000.

Table 1
Comparison of diameter measurement results for sample A by the three methods.

Inspection method	Average diameter (μm)	Actual diameter by ET3000 (μm)	RMSE (μm)
Proposed method	**3646.68**	**3647.52**	**7.72**
Fuzzy [18]	**3649.59**		**15.11**
ANFIS	**3650.42**		**10.31**

Table 2
Comparison of lens sag measurement results for sample A by the three methods.

Diameter data	Average lens sag (μm)	Actual lens sag by ET3000 (μm)	RMSE (μm)
Proposed method	**74.54**	**74.57**	**0.32**
Fuzzy [18]	**74.66**		**0.61**
ANFIS	**74.69**		**0.42**

The image resolution of the inspection system is 640 × 480. The system is supported with a 1–20X adjustable objective lens, a Manual Zoom lens and a 2X Adapter, where the actual length corresponding to a pixel can reach the micron level, thus, it can be applicable to the inspection of a large-size microlens.

In this study, three microlenses with different specifications are measured. The Surfcorder ET3000 (by KOSAKA Company) is employed to measure the above samples as a reference, and the diameter is measured by ET-3000 in the same direction as for all techniques. This instrument is a contact measurement device, which achieves point-to-point measurement of the object surface using a sharp probe with very high measurement precision. However, the probe may scratch the object surface, the instrument is very expensive, and the measurement speed is slow. Thus, this instrument is not suitable for in-line inspection. Therefore, the measurement results of ET-3000 are regarded as the actual specification value of the microlenses.

3.2. Measurement results of lens diameter and lens sag

The ANFIS model in Section 2.3 and the method proposed in literature [18] (Note: see the Appendix for the calculation process) are compared with the measurement results of the proposed sub-pixel algorithm. Since the ANFIS model and the method in literature [18] require much time to relearn the parameters of the different images, these methods are not suitable for the real

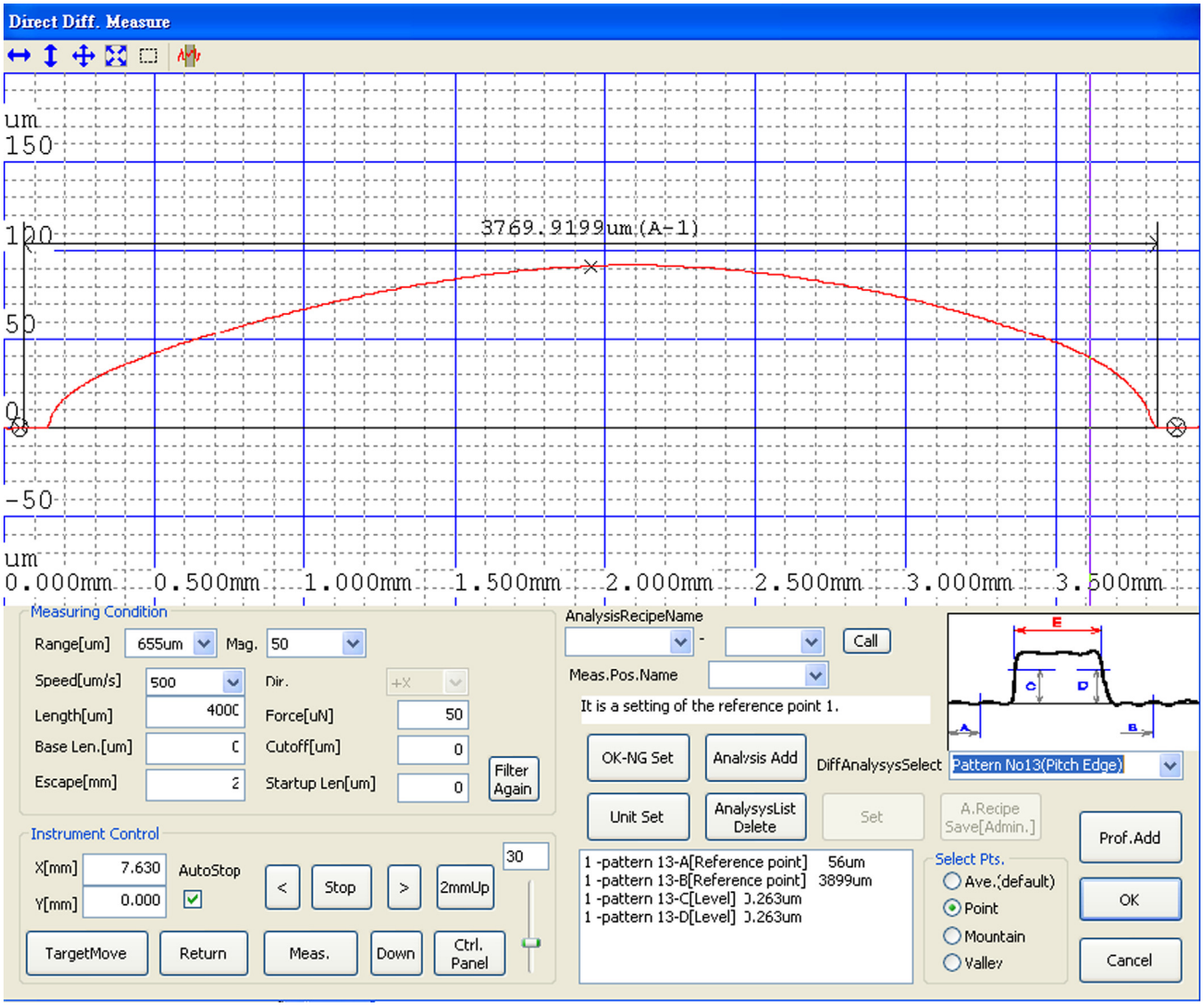

Fig. 13. Diameter measurement result of sample B by ET-3000.

Table 3
Comparison of diameter measurement results for sample B by the three methods.

Inspection method	Average diameter (μm)	Actual diameter by ET3000 (μm)	RMSE (μm)
Proposed method	**3769.39**	**3769.92**	**13.67**
Fuzzy [18]	**3775.12**		**19.34**
ANFIS	**3771.49**		**14.00**

Table 4
Comparison of lens sag measurement results for sample B by the three methods.

Diameter data	Average lens sag (μm)	Actual lens sag by ET3000 (μm)	RMSE (μm)
Proposed method	**92.15**	**92.18**	**0.67**
Fuzzy [18]	**92.43**		**0.95**
ANFIS	**92.25**		**0.69**

time inspection. The results of these methods serve the purpose of validating the robustness and practicability of the method described in Section 2.2.

The measured microlens samples can be divided into two groups according to their lens sag.

3.2.1. *Measurement of microlenses with large lens sag*

The diameters of microlens sample A and B are 3648 μm and 3770 μm, and their lens sags are 75 μm and 92 μm, which are far greater than the wavelength of light source. The backlight image and interference image are shown as Fig. 11(a) and (b).

Fifty diameters of sample A are measured, and Fig. 12 shows the diameter measurement result of sample A by ET-3000. The average diameter of the three methods is calculated respectively, and the Root Mean Square error (RMS error) of the three methods is also calculated:

$$\mathrm{RMSE} = \sqrt{\frac{(N_1-T)^2 + (N_2-T)^2 + \ldots + (N_{n_{rmse}}-T)^2}{n_{rmse}}} \tag{16}$$

where, Ni is the ith measurement result, T is the actual diameter, and n_{rmse} is the data number and is equal to 50 in this paper.

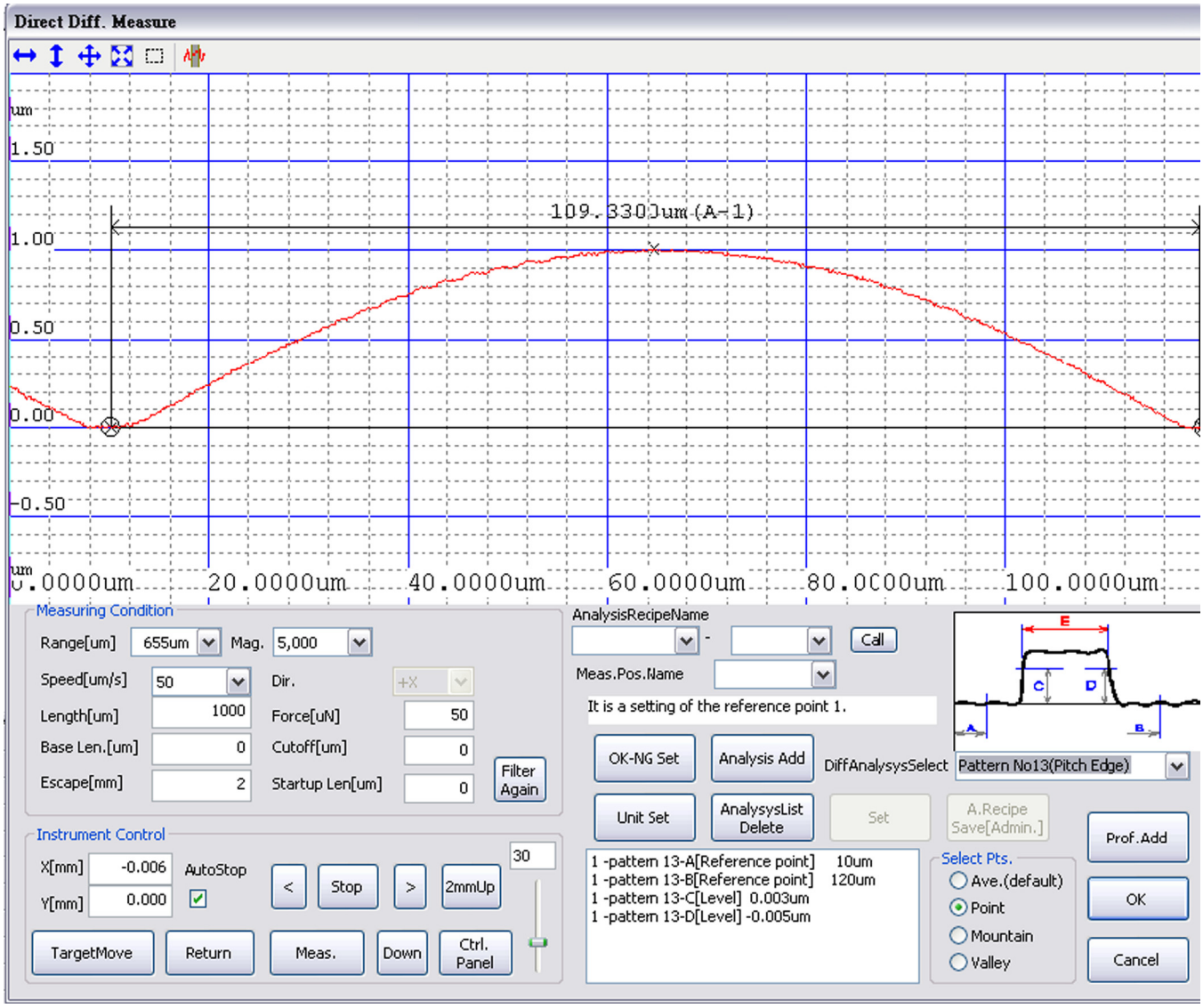

Fig. 14. Diameter measurement result of sample C by ET-3000.

Table 5
Comparison of diameter measurement results for sample C by the two methods.

Inspection method	Average diameter (μm)	Actual diameter by ET3000 (μm)	RMSE (μm)
Proposed method	**107.94**	**109.33**	**3.50**
ANFIS	**109.80**		**3.03**

Table 6
Comparison of lens sag measurement results for sample C by the two methods.

Diameter data	Average lens sag (μm)	Actual lens sag by ET3000 (μm)	RMSE (μm)
Proposed method	**1.02**	**0.99**	**0.06**
ANFIS	**1.06**		**0.08**

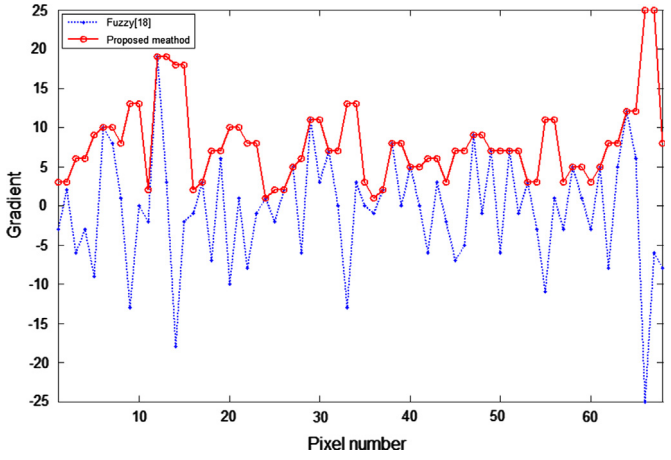

Fig. 15. Obtained gradients of the proposed method and literature [18] along an initiated ray.

Using the measurement result of ET-3000 as the actual diameter, and the comparison of diameter measurement results for sample A by the three methods is shown in Table 1

The lens sag of sample A is calculated by respectively substituting the 50 diameters measured using the three methods into Eq. (15). Table 2 shows the comparison results of the lens sag data.

Table A.1
Fuzzy rule table.

Rule (i)	Gradient	Gray value	ps (i)
1	$L_d(u)$	$L_g(w)$	pb (1)
2	$L_d(u)$	$\Pi_g(w)$	pm (2)
3	$L_d(u)$	$\Gamma_g(w)$	pm (3)
4	$\Pi_d(u)$	$L_g(w)$	ps (4)
5	$\Pi_d(u)$	$\Pi_g(w)$	ps (5)
6	$\Pi_d(u)$	$\Gamma_g(w)$	ps (6)
7	$\Gamma_d(u)$	$L_g(w)$	ps (7)
8	$\Gamma_d(u)$	$\Pi_g(w)$	ps (8)
9	$\Gamma_d(u)$	$\Gamma_g(w)$	ps (9)

The diameter of sample B is measured. Fig. 13 shows the diameter measurement result of sample B by ET-3000, and Table 3 shows the comparison results of the diameter data. The lens sag of sample B is calculated, and Table 4 shows the comparison results of the lens sag data.

3.2.2. *Measurement of microlenses with small lens sag*

The diameter of microlens sample C is 110 μm, and the lens sags is 1 μm, which is similarly equal to the wavelength of light source, as shown in Fig. 11(c). Since the fringe pattern of sample C is clearly distributed, the lens sag and lens diameter can be obtained through the conventional techniques [4–12]. However, this sample is still measured to verify the wild applicability of the proposed method.

The diameter of sample C is measured. Fig. 14 shows the diameter measurement result of sample C by ET-3000. Note that there are noises in the backlight image of sample C, and the contrast of edge points is lower when comparing with sample A and B. After testing, the method of literature [18] is not applicable for measuring the diameter of sample C. Hence, Tables 5 and 6 only show the comparison results of the diameter data and lens sag data by ANFIS model and sub-pixel algorithm.

3.3. *Discussion of measuring results*

As shown in Tables 1 and 3, the proposed sub-pixel algorithm can accurately measure the diameter of large-size microlens, the corresponding RMS error is less than 1% in diameter measurement, as compared with ET3000, and is the most accurate among the three methods. According to Tables 2 and 4, the more accurate the diameter measurement data are, the closer the lens sag is calculated as the actual value through Eq. (15). Compared with ET-3000, the RMS error is also less than 1% in lens sag measurement for large-size microlens, suggesting the accuracy of proposed method is good.

When measuring the diameter of sample C, the reason that the method of literature [18] is not applicable can be illustrated according to Fig. 15. Note that the definition of calculating gradient is different between the proposed method and literature [18], and there will be positive and negative values in the obtained gradients using the method of literature [18]. Since the grades of these negative gradients are judged as 0 by the defined membership function, the misjudgments of searching the edge points will therefore occur. In other words, the method of literature [18] is only suitable for the images with good contrast, low noises and uniform illumination. According to Tables 5 and 6, the RMS error is less than 6% for both diameter and lens sag measurement when comparing with ET-3000, showing that the proposed method is applicable for the microlenses with different sizes. However, it should be noted that the proposed method is not suitable for measuring the aspherical microlenses.

In general, the proposed sub-pixel algorithm is far simpler than the traditional LoG method, thus, the processing speed is significantly increased. Compared with ANFIS and literature [18], this method is characterized by high applicability, but without the need for prior training, and can be directly applied to different microlens images without manual sampling or substantial modification of the algorithm. In addition, this system has the architecture of non-contact measurement, which would not cause scratches on the microlens surface, and is particularly suitable for real time inspection of industry field.

4. Conclusions

An optical inspection system is successfully proposed in this study for measuring the diameter and lens sag of large-size microlenses. As the contrast ratio of a large-size microlens edge is very low, resulting in very fuzzy edge areas in an image, and the microlens diameter is unable to be directly determined. Therefore, after identifying the central position of a microlens, an automatic sub-pixel algorithm is proposed in this study to accurately determine the edge points of a microlens and measure microlens diameter. The proposed method can improve the complex computations of the traditional LoG method, and is characterized by good accuracy, high applicability, and rapid processing speed, but without the need for prior training, as compared with ANFIS and other methods. By integrating the diameter measurement algorithm, a rule is also proposed to estimate lens sag, which is characterized by high measurement speed and non-contact structure, would not cause scratches on the microlens surface, and is particularly suitable for the in-line inspection of industry field.

Acknowledgment

This work is sponsored by the National Science Council under Grant No. NSC 100-2221-E-009-024.

Appendix

The membership functions of gradient and gray value in the literature [18] are redefined in this paper for searching the edge points of a large-size microlens. The membership functions of the gradient are modified as $L_d(u)$, $\Pi_d(u)$and $\Gamma_d(u)$, where u represents the gradient

$$L_d(u)=\begin{cases}1, & u<30\\ 1-\frac{u-30}{50-30}, & 30\le u\le 50\\ 0, & u>50\end{cases} \tag{A.1}$$

$$\Pi_d(u)=\begin{cases}0, & u<40\\ \frac{u-40}{50-40}, & 40\le u<50\\ 1, & 50\le u\le 70\\ 1-\frac{u-70}{80-70}, & 70<u\le 80\\ 0, & u>80\end{cases} \tag{A.2}$$

$$\Gamma_d(u)=\begin{cases}0, & u<70\\ \frac{u-70}{90-70}, & 70\le u\le 90\\ 1, & u>90\end{cases} \tag{A.3}$$

The membership functions of the gray value as $L_g(w)$, $\Pi_g(w)$ and $\Gamma_g(w)$ are also modified, where w represents the gray value

$$L_g(w)=\begin{cases}1, & w<100\\ 1-\frac{w-100}{140-100}, & 100\le w\le 140\\ 0, & w>140\end{cases} \tag{A.4}$$

$$\Pi_g(w)=\begin{cases}0, & w<130\\ \frac{w-130}{140-130}, & 130\le w<140\\ 1, & 140\le w\le 160\\ 1-\frac{w-160}{170-160}, & 160<w\le 170\\ 0, & w>170\end{cases} \tag{A.5}$$

$$\Gamma_g(w)=\begin{cases}0, & w<160\\ \frac{w-160}{180-160}, & 160\le w\le 180\\ 1, & w>180\end{cases} \tag{A.6}$$

The corresponding fuzzy rule table is defined as Table A.1. After the defuzzification, the pixel with the highest possibility is the edge point of the microlens, and the diameter of microlens can be calculated using Eq. (10).

References

[1] Bogner A, Jouneau PH, Thollet G, Basset D, Gauthier C. A history of scanning electron microscopy developments: towards wet-STEM imaging. Micron 2007;38(4):390–401.

[2] Zhong ZW, Lu YG. Measurements of surface deformations and strains using an AFM moiré method. Measurement 2005;38(1):34–41.

[3] Badami VG, Smith ST, Raja J, Hocken RJ. A portable three-dimensional stylus profile measuring instrument. Precision Engineering 1996;18(2–3):147–56.

[4] Lin CS, Loh GH, Fu SH, Yang SW, Chang HK, Yeh MS. An automatic evaluation method for the surface profile of the microlens array using an optical interferometric microscope. Measurement Science and Technology 2010;21 (11):1–10 105304.

[5] Zhao H, Liang R, Li D, Cao M. Practical common-path heterodyne surface profiling interferometer with automatic focusing. Optics and Laser Technology 2001;33(4):259–65.

[6] Yang SW, Lin CS, Lin SK. 3D surface profile measurement of unsymmetrical microstructure using fizeau interferometric microscope. Optics and Lasers in Engineering 2013;51(4):348–57.

[7] Chatterjee S, Kumar YP, Bhaduri B. Measurement of surface figure of plane optical surfaces with polarization phase-shifting Fizeau interferometer. Optics and Laser Technology 2007;39:268–74.

[8] Lin CS, Lin CH, Lin CC, Yeh MS. Three-dimensional profile measurement of small lens using subpixel localization with color grating. Optik 2010;121 (23):2122–7.

[9] Zhang Q, Wang Q, Hou Z, Liu Y, Su X. Three-dimensional shape measurement for an underwater object based on two-dimensional grating pattern projection. Optics and Laser Technology 2011;43(4):801–5.

[10] Thakur M, Quan C, Tay CJ. Surface profiling using fringe projection technique based on Lau effect. Optics and Laser Technology 2007;39(3):453–9.

[11] Quan C, Shang HM, Bryanston-Cross PJ. Application of the holographic carrier fringe and FFT technique for deformation measurement. Optics and Laser Technology 1996;28(1):7–13.

[12] Tien CL, Lin YN, Sun WS, Lin TW, Lin CS, Zhang JY. Design and evaluation of aspherical microlens module for high speed data transmission. Optics and Precision Engineering 2011;19(9):2271–6.

[13] Yang SW, Lin CS, Fu SH, Yeh MS, Tsou C, Lai TH. Lens sag measurement of microlens array using optical interferometric microscope. Optics Communications 2012;285(6):1066–74.

[14] Zeng J, Li D. Color image edge detection method using VTV denoising and color difference. Optik 2012;123(22):2072–5.

[15] Wu J, Yin ZP, Xiong YL. The fast multilevel fuzzy edge detection of blurry images. IEEE Signal Processing Letters 2007;14(5):344–7.

[16] Ville DVD, Nachtegael M, Weken DV, Kerre EE, Philips W, Lemahieu I. Noise reduction by fuzzy image filtering. IEEE Transactions on Fuzzy Systems 2003;11(4):429–36.

[17] Law T, Itoh H, Seki H. Image filtering, edge detection, and edge tracing using fuzzy reasoning. IEEE Transactions on Pattern Analysis and Machine Intelligence 1996;18(5):481–91.

[18] CS Lin, GH Loh, CL Tien, TC Lin, YC Chiou, Automatic optical inspection system for the micro-lens of optical connector with fuzzy ratio analysis, OPTIK, http://dx.doi.org/10.1016/j.ijleo.2012.09.058, in press.

[19] Cheng SC, Wu TL. Subpixel edge detection of color images by principal axis analysis and moment-preserving principle. Pattern Recognition 2005;38: 527–37.

[20] Cielo P, Vaudreuil G. Algorithm for subpixel edge positioning and part sizing under coherent projection. Optics and Laser Technology 1991;23(2):85–97.

[21] Jang JS. ANFIS: adaptive network-based fuzzy inference system. IEEE Transactions on Systems, Man, and Cybernetics 1993;23(3):665–86.

[22] Marr D, Hildreth E. Theory of edge detection. Proceedings of the Royal Society of LondonSeries B: Biological Sciences 1980;207(1167):187–217.